



Article

Effect of Nano-Y₂O₃ Content on Microstructure and Mechanical Properties of Fe₁₈Cr Films Fabricated by RF Magnetron Sputtering

Bang-Lei Zhao^{1,2}, Le Wang^{3,4}, Li-Feng Zhang^{1,2}, Jian-Gang Ke^{1,2}, Zhuo-Ming Xie¹, Jun-Feng Yang^{1,5,*} , Xian-Ping Wang¹, Ting Hao⁶, Chang-Song Liu^{1,*} and Xue-Bang Wu¹ 

- ¹ Key Laboratory of Materials Physics, Institute of Solid State Physics, HFIPS, Chinese Academy of Sciences, Hefei 230031, China; zbl1234@mail.ustc.edu.cn (B.-L.Z.); zlf05358@mail.ustc.edu.cn (L.-F.Z.); jingkej@126.com (J.-G.K.); zmxie@issp.ac.cn (Z.-M.X.); xpwang@issp.ac.cn (X.-P.W.); xbwu@issp.ac.cn (X.-B.W.)
- ² University of Science and Technology of China, Hefei 230026, China
- ³ Beijing Institute of Technology Chongqing Innovation Center, Chongqing 401135, China; wangle@bit.edu.cn
- ⁴ School of Materials Science and Engineering, Beijing Institute of Technology, Beijing 100081, China
- ⁵ Lu'an Branch, Anhui Institute of Innovation for Industrial Technology, Lu'an 237100, China
- ⁶ School of Mechanical Engineering, Suzhou University of Science and Technology, Suzhou 215009, China; hao.ting@mail.usts.edu.cn
- * Correspondence: jfyang@issp.ac.cn (J.-F.Y.); cslu@issp.ac.cn (C.-S.L.)



Citation: Zhao, B.-L.; Wang, L.; Zhang, L.-F.; Ke, J.-G.; Xie, Z.-M.; Yang, J.-F.; Wang, X.-P.; Hao, T.; Liu, C.-S.; Wu, X.-B. Effect of Nano-Y₂O₃ Content on Microstructure and Mechanical Properties of Fe₁₈Cr Films Fabricated by RF Magnetron Sputtering. *Nanomaterials* **2021**, *11*, 1754. <https://doi.org/10.3390/nano11071754>

Academic Editor: Marcela Achimovičová

Received: 26 May 2021
Accepted: 1 July 2021
Published: 5 July 2021

Publisher's Note: MDPI stays neutral with regard to jurisdictional claims in published maps and institutional affiliations.



Copyright: © 2021 by the authors. Licensee MDPI, Basel, Switzerland. This article is an open access article distributed under the terms and conditions of the Creative Commons Attribution (CC BY) license (<https://creativecommons.org/licenses/by/4.0/>).

Abstract: In this work, FeCr-based films with different Y₂O₃ contents were fabricated using radio frequency (RF) magnetron sputtering. The effects of Y₂O₃ content on their microstructure and mechanical properties were investigated through scanning electron microscopy (SEM), transmission electron microscopy (TEM), X-ray photoelectron spectroscopy (XPS), inductive coupled plasma emission spectrometer (ICP) and a nanoindenter. It was found that the Y₂O₃-doped FeCr films exhibited a nanocomposite structure with nanosized Y₂O₃ particles uniformly distributed into a FeCr matrix. With the increase of Y₂O₃ content from 0 to 1.97 wt.%, the average grain size of the FeCr films decreased from 12.65 nm to 7.34 nm, demonstrating a grain refining effect of Y₂O₃. Furthermore, the hardness of the Y₂O₃-doped FeCr films showed an increasing trend with Y₂O₃ concentration, owing to the synergetic effect of dispersion strengthening and grain refinement strengthening. This work provides a beneficial guidance on the development and research of composite materials of nanocrystalline metal with a rare earth oxide dispersion phase.

Keywords: FeCr-based films; oxide dispersion strengthening; nanoindentation hardness

1. Introduction

The discovery and application of nuclear energy are regarded as two of the most important scientific and technological achievements of the twentieth century. As a kind of clean and sustainable energy, nuclear energy can extensively replace conventional fossil energy [1,2]. So far, the studies on nuclear energy systems have made great progress, but material issue is still one of the key challenges that restrict the development of nuclear energy [3–6]. In particular, for future advanced nuclear reactors, such as fast reactors [7], thermonuclear fusion reactors (TFR) [8] and accelerator driven sub-critical systems (ADS) [9], due to their severely harsh service environment which includes a high temperature, strong irradiation and strong corrosion, materials with superior service performance and reliability are urgently needed.

FeCr-based steels have been widely considered as one of the most important structure materials for nuclear reactors because of their outstanding mechanical properties. However, in the long-term nuclear service process, FeCr-based structural alloys, such as 304 and 316 stainless steel, have to bear high-dose irradiation damages, which accordingly induce

irradiation hardening [5], porosity evolution and swelling [10], high temperature helium embrittlement (HTHE) [11], etc. Therefore, how to increase the irradiation resistance of FeCr-based alloys is still a key problem to be solved until now. Oxide dispersion-strengthened (ODS) steels are a great development in nuclear energy structure materials, owing to their excellent irradiation resistance property [12,13]. S. Ukai et al. found that nanoparticles could act as sinks for the trapping of helium atoms and point defects, thus retarding radiation-induced material degradation [14]. Moreover, FeCr alloys with the addition of oxide particles have been shown to have high tensile, creep and fatigue strength, have thermal stability through the promotion of radiation-induced defect recombination, trap He atoms and impede dislocation climb and glide [15]. In particular, the addition of a small amount of Y_2O_3 nanoparticles (0.1~0.5 wt.%) in the alloy matrix can not only improve its mechanical properties, but also annihilate the defects effectively caused by irradiation [16–19]. Moreover, the grain refinement of structural materials is also treated as one of the effective methods of optimizing the strength and irradiation resistance properties, owing to the high density of interface, especially in nanocrystalline materials, as reported in nanocrystalline Au (grain size~23 nm) [20] and TiNi alloys (grain size 23–31 nm) [21]. This is because the high-density interface in nanocrystalline materials can effectively absorb and annihilate the irradiation defects, which shows a better anti-irradiation performance than that of coarse grain materials. Meanwhile, an increase in the strength of nanostructured materials has been achieved over the last several decades based on extrapolations of the grain size dependence of mechanical properties of conventional materials [22]. The general enhancement in the materials' strength is dependent on the grain size, which is often described by the empirical Hall–Petch relationship [23].

Magnetron sputtering is known as one of the most useful methods of fabricating nanocrystalline materials [24–27], in which grain size, density and film thickness can be well controlled through adjusting the sputtering parameters, such as substrate temperature, sputtering power, sputtering time and sputtering pressure. It is known that thin films and bulks materials have different application fields. The thin films cannot be used as the construction materials of nuclear reactors. However, the FeCr-based thin films can be adopted as a platform to model the nanocrystalline metal materials with an extremely high volume fraction of grain boundaries, and to investigate the mechanism of Y_2O_3 -induced strengthening. Therefore, in this work, the magnetron sputtering ODS-FeCr films were prepared and researched in order to provide a beneficial guidance for the research and development of fission reactor structural materials in the future.

2. Experimental

Composite targets composed of $Fe_{18}Cr$ -based steel holder and Y_2O_3 slices were designed (Figure 1a). By changing the number of Y_2O_3 slices, the Y_2O_3 contents could be adjusted in the deposited film. Si single crystal wafers with (111) orientation were used as substrates. Y_2O_3 -doped FeCr films were fabricated by radio frequency (RF) magnetron sputtering technique. The rotating target was used in this deposition experiment to guarantee the homogeneous distribution of chemical elements in the films. There was an annular magnetic field around the target and the electrons moved in a cycloid-like manner on the surface of the target. Before sputtering, the vacuum chamber was evacuated to 8.0×10^{-4} Pa by a molecular pump, and then the working argon (Ar) gas was filled into the chamber and the working pressure was kept at about 1.0 Pa. The sputtering time was 4 h, the sputtering power was controlled at 70 W and the substrate temperature was fixed at 200 °C.

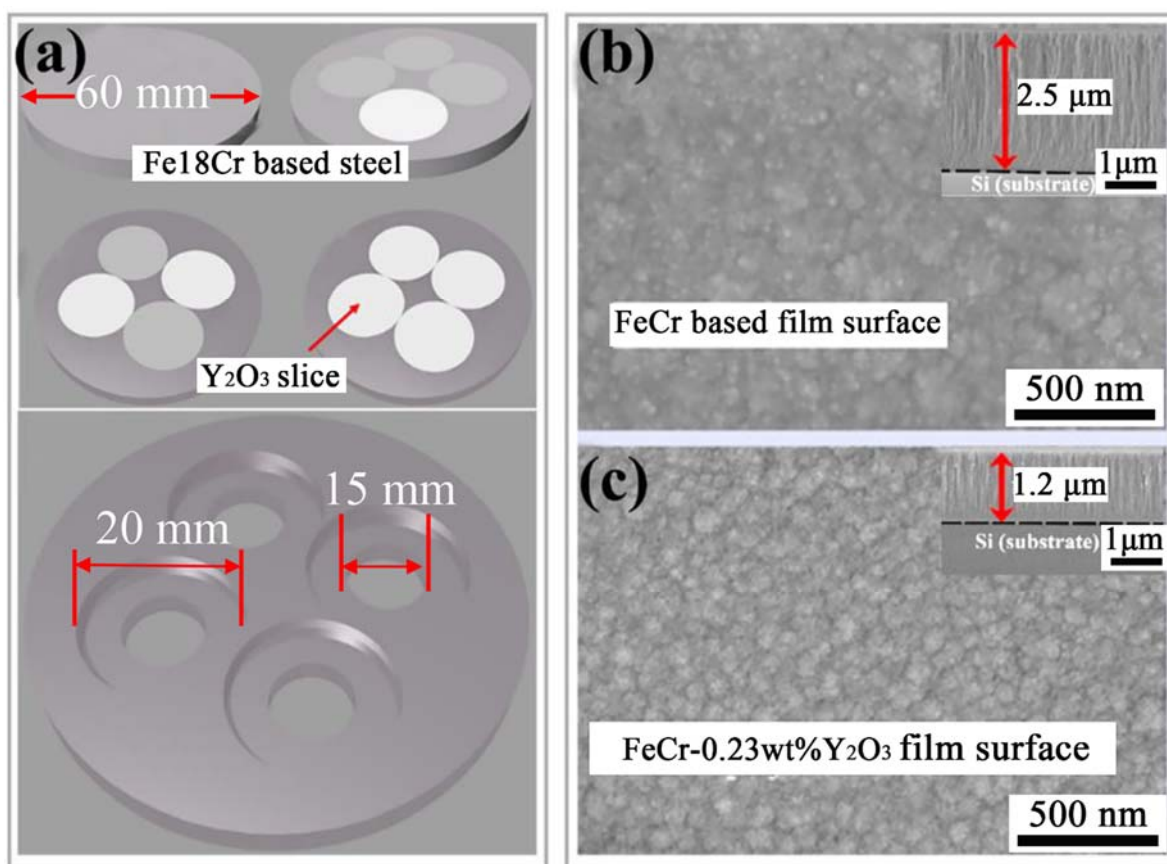


Figure 1. (a) Schematic of Y_2O_3 /FeCr steel composited targets. White: Y_2O_3 slice; Dark: Fe/Cr metals slice; (b,c) surface and cross-section morphology of pure FeCr films with and without Y_2O_3 addition.

The crystalline structure of the films was characterized using a grazing incident X-ray diffractometer (GIXRD, PANalytical Company, Netherlands, Philips X'pert PRO, $Cu K\alpha$ radiation, wavelength ~ 0.15418 nm) with a step size of 0.06° and grazing angle of 1.5° . The surface and cross-section morphology of the films were observed by field emission scanning electron microscopy (FESEM, Sirion 200FEG, HITACHI, Japan, accelerating voltage 5 keV) with equipment of a secondary electron detector. Observations of Y_2O_3 in the as-deposited films were operated by a transmission electron microscopy (TEM, Tecnai TF20 TMP, Gatan Company USA) with an accelerating voltage of 200 kV. Cross-sectional TEM samples were prepared by a method combining the methods of mechanical thinning with Ar ion milling.

Microhardness tests were carried out on surface of the films by the nanoindentation (Nano-indenter G200, Agilent, USA) with a strain rate of $0.05 s^{-1}$. The average hardness values were calculated from 15 separate indents with the depth range of 200–500 nm.

3. Results and Discussion

In order to investigate the effects of Y_2O_3 addition on the microstructure and mechanical properties of FeCr films, Y_2O_3 /FeCr composite targets with 0, 1, 2 and 4 pieces of Y_2O_3 slices were used during sputtering (Figure 1a), and the resultant films were designated as FeCr, Y_2O_3 -FeCr, $2Y_2O_3$ -FeCr, $4Y_2O_3$ -FeCr, respectively, herein. The concentration of Y_2O_3 in the FeCr films was analyzed by the inductive coupled plasma emission spectrometer (ICP), as shown in Table 1. It can be seen that as the number of Y_2O_3 slices is 0, 1, 2 and 4, the Y_2O_3 content is 0, 0.12, 0.23 and 1.97 wt.%, respectively. The abnormal increase of Y contents from 0.23 to 1.97 as the Y_2O_3 slice number increase from 2 to 4 was difficult to understand in terms of the sputtering area of the Y_2O_3 slice, but was tentatively attributed to the change in glow discharge mode induced by the Y_2O_3 .

Table 1. Y_2O_3 content, thickness and coherent domain size of Y_2O_3 -doped FeCr films sputter deposited from FeCr target incorporated with 1, 2 and 4 pieces of Y_2O_3 slices, respectively.

Materials (Y_2O_3 Slices)	Y_2O_3 Content wt.%	Y_2O_3 Content at%	Thickness (μm)	Coherent Domain Size (nm)
0	0	0	2.5	12.65 ± 0.82
1	0.12	0.08	1.5	10.86 ± 0.94
2	0.23	0.14	1.2	9.63 ± 0.23
4	1.97	1.01	1.0	7.34 ± 0.25

Figure 1b,c show the surface and cross-section morphology of pure FeCr films and $2Y_2O_3$ -FeCr films, respectively. The large columnar crystal consisting of small columnar nanocrystals was observed in both the pure and $2Y_2O_3$ -FeCr films. For the $2Y_2O_3$ -FeCr film (Figure 1c), the number of grains per unit area was denser compared with that of the pure FeCr film (Figure 1b). In addition, the film thickness of the FeCr, Y_2O_3 -FeCr, $2Y_2O_3$ -FeCr and $4Y_2O_3$ -FeCr films were 2.5, 1.5, 1.2, 1.0 μm , respectively, showing a decreasing trend with the increasing number of Y_2O_3 slice as shown in Table 1. The reason is that under the same sputtering conditions, the sputtering yield of Y_2O_3 ceramic is lower than that of the FeCr metal in the composite target.

Figure 2a shows the XRD patterns of FeCr-based films with four kinds of Y_2O_3 contents. All films exhibit the typical cubic ferrite phase structure, but the Y_2O_3 -related diffraction peaks were not observed owing to their extremely low concentrations below the detecting limit of the XRD instrument. Based on the Scherrer equation $D = k\lambda / B\cos\theta$, where D is the coherent domain size, k is constant, B is the full width at half maximum (FWHM) and θ is the diffraction angle, the coherent domain size was roughly evaluated as about 7~12 nm (shown in Table 1) in terms of the FWHM of the (110) main diffraction peaks. It is worth pointing out that the coherent domain size D has a gradually decreasing tendency with an increase in Y_2O_3 content, which implies the grain refinement effect of Y_2O_3 . This demonstrates that magnetron sputtering is a powerful technique for the preparation of ODS-nanocrystalline metal thin films.

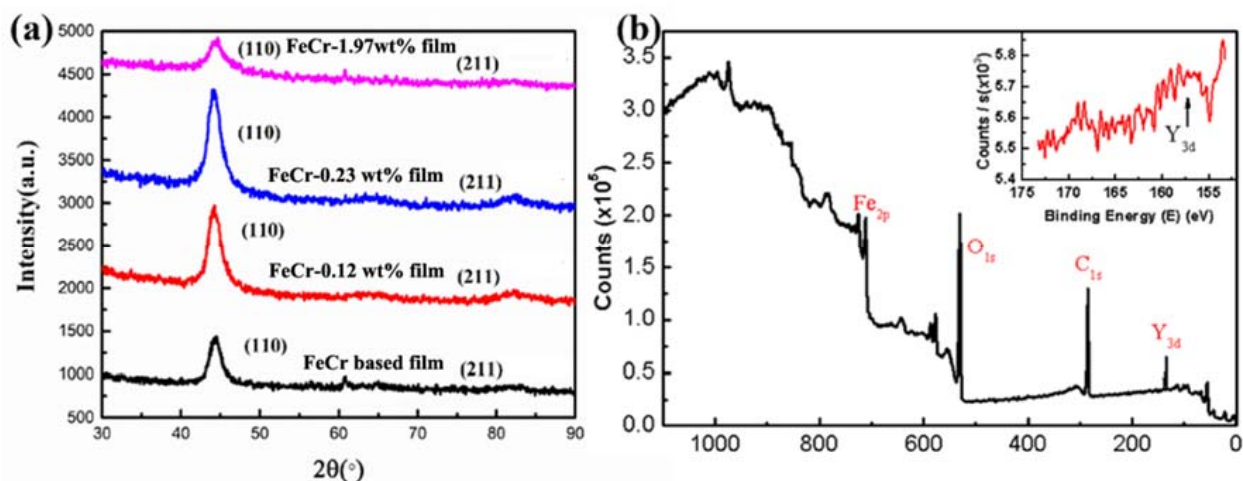


Figure 2. (a) X-ray diffraction patterns of FeCr films with different Y_2O_3 content; (b) XPS spectrum of $2Y_2O_3$ -FeCr (0.12 wt.% Y_2O_3) film.

To confirm the formation of the Y_2O_3 , the XPS (X-ray photoelectron spectroscopy) analysis was conducted. As shown in Figure 2b, a specific electron binding energy was found to coincide with the energy value of $Y_{3d5/2}$ electrons in molecular Y_2O_3 . This result indicates that the Y elements exist in the form of Y_2O_3 in fabricated films, which is in line with the expectation of realizing oxide dispersion strengthening in FeCr based films by radio frequency magnetron sputtering (RFMS) methods.

Figure 3 displays the elemental distribution of the Fe, Cr, Y and EDS (Energy Dispersive Spectroscopy) spectrum of the $4\text{Y}_2\text{O}_3\text{-FeCr}$ film. The EDS mapping shows that all elements (Fe, Cr and Y) on the surface of the film are evenly distributed, though the signal of Y is weak due to the low content of Y, which is close to background level. The concentration of Ar is negligible, although argon is used as the working gas. The EDS spectrum obtained from the cross-section of the $4\text{Y}_2\text{O}_3\text{-FeCr}$ film in the line scanning mode demonstrates the existence of 1.58 wt.% Y and 0.42 wt.% O, corresponding to 2.0 wt.% Y_2O_3 in the film. In order to clarify how the element Y existed, the microstructures of pure FeCr and FeCr-0.23 wt.% Y_2O_3 were characterized using TEM and high-resolution TEM (HRTEM), as shown in Figure 4a–c. A large amount of nano-scale Y_2O_3 particles of 5–10 nm in diameter are uniformly dispersed in the volume of the FeCr-based films (Figure 4b). Based on the diffraction fringes in the high-resolution TEM (HRTEM) image of FeCr-0.23 wt.% Y_2O_3 (Figure 4c), the crystalline interplanar spacings are determined as 0.146 and 0.238 nm, in accordance with the (320) and (210) crystal plane of the cubic structure Y_2O_3 with the space group Ia3 (PCPDF card: 00-025-1200). These uniformly distributed Y_2O_3 nanoparticles would significantly strengthen the FeCr films.

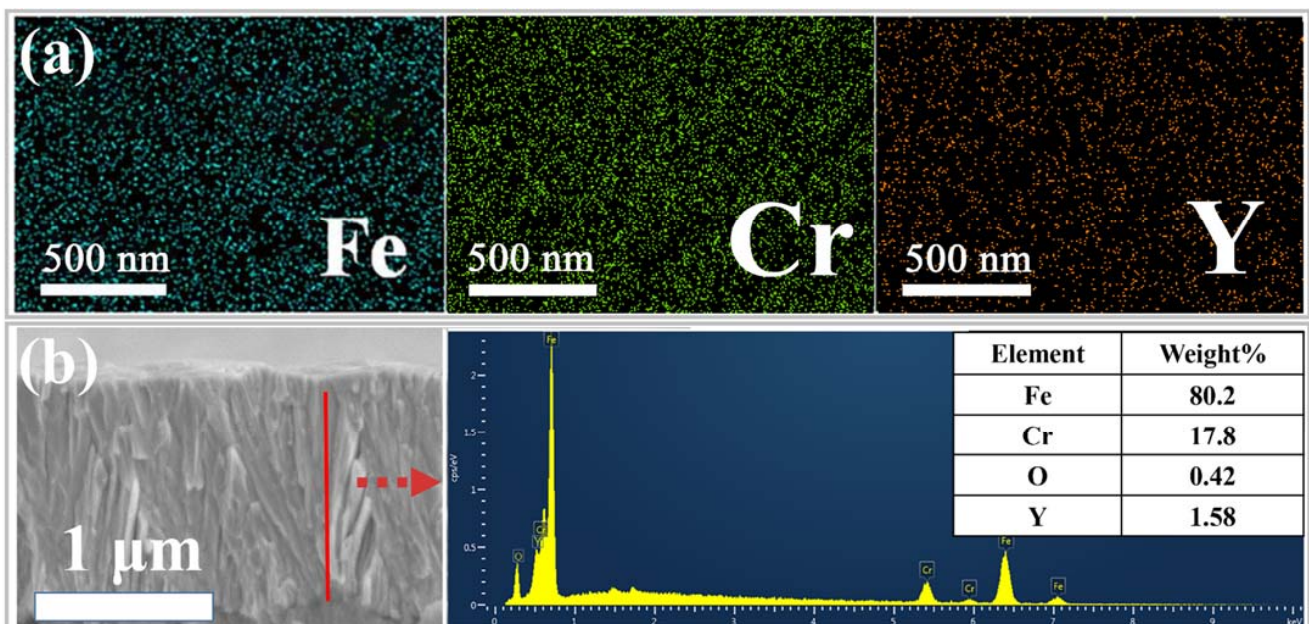


Figure 3. (a) 2D elemental mapping of Fe, Cr and Y in ODS-FeCr-based films prepared through sputtering FeCr target with 2 slices of Y_2O_3 , (b) cross-section morphology and the corresponding EDS spectrum of FeCr-based films prepared through sputtering FeCr target with 4 slices of Y_2O_3 .

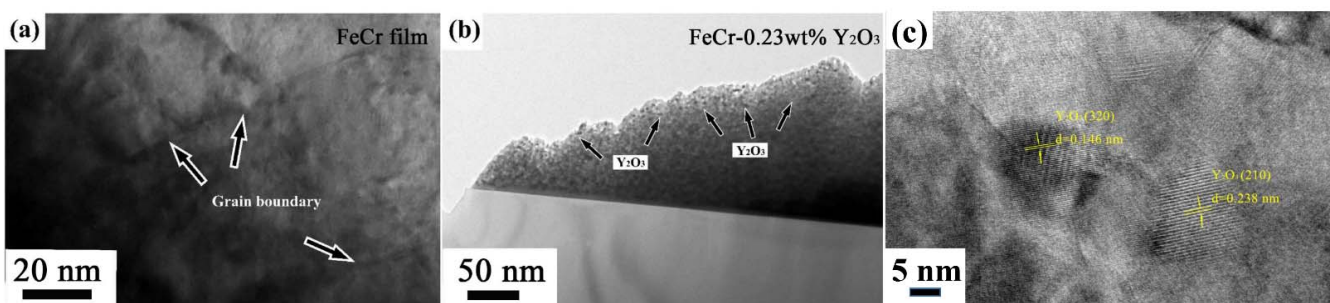


Figure 4. (a) Cross-sectional TEM images of FeCr films; (b) FeCr-0.23wt.% Y_2O_3 ; (c) HRTEM image of FeCr-0.23wt.% Y_2O_3 .

A nanoindenter technique was used to explore the microhardness of these ODS-FeCr-based films. Figure 5a displays the hardness vs. displacement curves of the FeCr-

based films with different Y_2O_3 contents. The indentation depth h was controlled in the range of 0 to 500 nm in order to exclude the influence of the Si substrate. The effective nanoindentation hardness of the ODS-FeCr-based films deposited under different Y_2O_3 concentrations was calculated by averaging the relatively stable platform of hardness–depth profiles located in 100–500 nm, as shown in Figure 5b. It can be seen that the film hardness distinctly increases with the increase of the Y_2O_3 concentration, and the hardness value increases from 10.4 GPa to 16.5 GPa, exhibiting the obvious nano-oxide dispersion strengthened effect. Song et al. [27] raised an Orowan model demonstrating that the moving dislocation lines can be markedly hindered by the oxide particle. In the present Y_2O_3 -doped FeCr films, the uniformly distributed nano Y_2O_3 particles act as an obstacle for the dislocation motion during deformation, which is beneficial for improving the mechanical property. Moreover, grain refining is another way to increase the hardness of hard films. Wang et al. demonstrated that the hardness (H) of a metallic material increases with a decreasing grain size d , according to the Hall–Petch relation $H = H_0 + kd^{-1/2}$ (k is constant) [28,29]. Grain refinement increased the number of grain boundaries, which improved the obstacle to material deformation and dispersed the stress concentration. Based on the analysis above, the extremely high hardness of Y_2O_3 -doped FeCr films is attributed to the synergetic strengthen effect of dispersion strengthening and grain refinement strengthening.

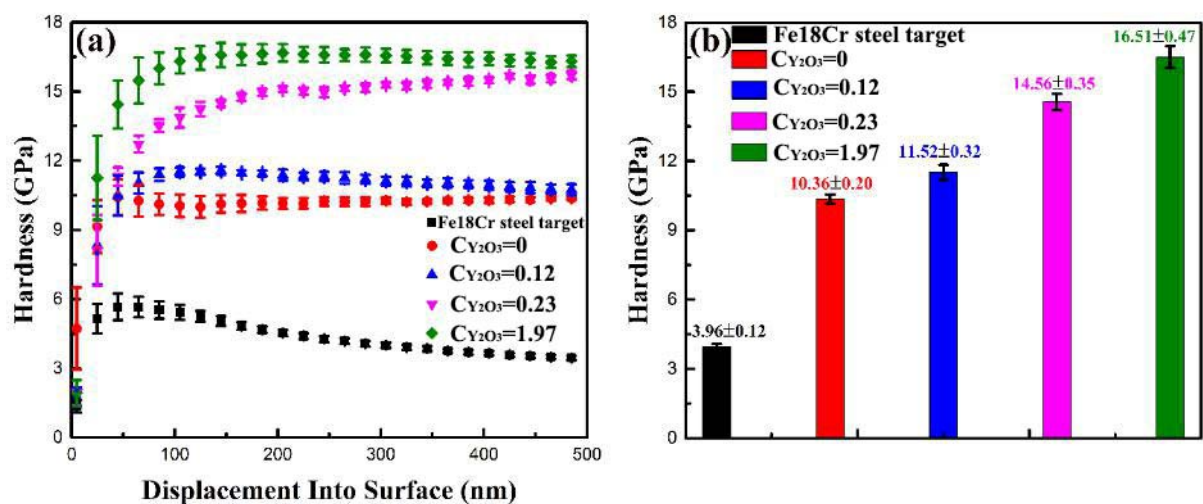


Figure 5. (a) Nanoindentation hardness (H)-depth (h) curves of the FeCr-based sheet and FeCr-based films with different Y_2O_3 content; (b) Hardness of the FeCr-based steel sheet and FeCr-based films with different Y_2O_3 concentration.

4. Conclusions

Y_2O_3 -dispersed FeCr films were grown through a RF magnetron sputtering technique and the effects of Y_2O_3 addition on their microstructures and hardness were thoroughly investigated. The main results can be concluded as follows:

- (1) The coherent domain size of ODS-FeCr-based film is about 7~12 nm, and it decreases with an increase in Y_2O_3 content.
- (2) The addition of Y_2O_3 can obviously enhance the hardness of FeCr-based films, resulting in an extremely high value of 16.5 GPa.
- (3) The strengthening mechanism was from the nano- Y_2O_3 particle dispersion strengthening as well as the grain refinement strengthening.

Author Contributions: B.-L.Z.: Methodology, Investigation, Data Curation, Writing-Original Draft. L.W.: Conceptualization. L.-F.Z.: Investigation, Data Curation. J.-G.K.: Investigation, Data Curation. Z.-M.X.: Methodology, Investigation, Data Curation. J.-F.Y.: Project administration, Funding acquisition, Writing-Review & Editing. X.-P.W.: Investigation. T.H.: Investigation, Data Curation. C.-S.L.:

methodology. X.-B.W.: Review & Editing. All authors have read and agreed to the published version of the manuscript.

Funding: This work was supported by the National Natural Science Foundation of China (Grant Nos. 11735015, 51771181, 51971212, 11755255), The Fund of Science and Technology on Reactor Fuel and Materials Laboratory (Grant No. 6142A06200310).

Institutional Review Board Statement: Not applicable.

Informed Consent Statement: Not applicable.

Data Availability Statement: The data that support the findings of this study are available from the corresponding author, [author initials], upon reasonable request.

Conflicts of Interest: The authors declare no conflict of interest.

References

1. Zinkle, S.J. Challenges in Developing Materials for Fusion Technology—Past, Present and Future. *Fusion Sci. Technol.* **2013**, *64*, 65–75. [[CrossRef](#)]
2. Mansur, L.; Rowcliffe, A.; Nanstad, R.; Zinkle, S.; Corwin, W.; Stoller, R. Materials needs for fusion, Generation IV fission reactors and spallation neutron sources—similarities and differences. *J. Nucl. Mater.* **2004**, *329*, 166–172. [[CrossRef](#)]
3. Beeler, B.; Asta, M.; Hosemann, P.; Grønbech-Jensen, N. Effects of applied strain on radiation damage generation in body-centered cubic iron. *J. Nucl. Mater.* **2015**, *459*, 159–165. [[CrossRef](#)]
4. Judge, C.D.; Gauquelin, N.; Walters, L.; Wright, M.; Cole, J.I.; Madden, J.; Botton, G.A.; Griffiths, M. Intergranular fracture in irradiated Inconel X-750 containing very high concentrations of helium and hydrogen. *J. Nucl. Mater.* **2015**, *457*, 165–172. [[CrossRef](#)]
5. Zhang, H.; Zhang, C.; Yang, Y.; Meng, Y.; Jang, J.; Kimura, A. Irradiation hardening of ODS ferritic steels under helium implantation and heavy-ion irradiation. *J. Nucl. Mater.* **2014**, *455*, 349–353. [[CrossRef](#)]
6. Gao, C.; Doyle, W.D.; Shamsuzzoha, M. Quantitative correlation of phase structure with the magnetic moment in rf sputtered Fe-N films. *J. Appl. Phys.* **1993**, *73*, 6579–6581. [[CrossRef](#)]
7. Little, E.A.; Stow, D.A. Void-swelling in irons and ferritic steels_ II. An experimental survey of materials irradiated in a fast reactor. *J. Nucl. Mater.* **1979**, *87*, 25–39. [[CrossRef](#)]
8. Group, T. Pump limiter experiment in the TFR Tokamak. *J. Nucl. Mater.* **1987**, *145*, 819–823.
9. Kapoor, S.S. Accelerator-driven sub-critical reactor system (ADS) for nuclear energy generation. *Indian Acad. Sci.* **2002**, *59*, 941–950. [[CrossRef](#)]
10. Trinkaus, H.; Singh, B.N. Helium accumulation in metals during irradiation—Where do we stand? *J. Nucl. Mater.* **2003**, *323*, 229–242. [[CrossRef](#)]
11. Hasegawa, A.; Ejiri, M.; Nogami, S.; Ishiga, M.; Kasada, R.; Kimura, A.; Abe, K.; Jitsukawa, S. Effects of helium on ductile-brittle transition behavior of reduced-activation ferritic steels after high-concentration helium implantation at high temperature. *J. Nucl. Mater.* **2009**, *386*, 241–244. [[CrossRef](#)]
12. de Castro, V.; Leguey, T.; Monge, M.; Munoz, A.; Pareja, R.; Amador, D.; Torralba, J.; Victoria, M. Mechanical dispersion of Y₂O₃ nanoparticles in steel EUROFER 97: Process and optimization. *J. Nucl. Mater.* **2003**, *322*, 228–234. [[CrossRef](#)]
13. Ukai, S.; Kaito, T.; Ohtsuka, S.; Narita, T.; Fujiwara, M.; Kobayashi, T. Production and properties of nano-scale oxide dispersion strengthened (ODS) 9Cr martensitic steel claddings. *ISIJ Int.* **2003**, *43*, 2038–2045. [[CrossRef](#)]
14. Ukai, S.; Fujiwara, M. Perspective of ODS alloys application in nuclear environments. *J. Nucl. Mater.* **2002**, *307–311*, 749–757. [[CrossRef](#)]
15. Bhattacharyya, D.; Dickerson, P.; Odette, G.R.; Maloy, S.A.; Misra, A.; Nastasi, M.A. On the structure and chemistry of complex oxide nanofeatures in nanostructured ferritic alloy U14YWT. *Philos. Mag.* **2012**, *92*, 2089–2107. [[CrossRef](#)]
16. Liu, X.; Yin, H.; Xu, Y. Microstructure, mechanical and tribological properties of oxide dispersion strengthened high-entropy alloys. *Materials* **2017**, *10*, 1312. [[CrossRef](#)] [[PubMed](#)]
17. Aguirre, M.V.; Martín, A.; Pastor, J.Y.; Lorca, J.L.; Monge, M.A.; Pareja, R. Mechanical properties of Y₂O₃-doped W–Ti alloys. *J. Nucl. Mater.* **2010**, *404*, 203–209. [[CrossRef](#)]
18. Hu, W.; Sun, T.; Liu, C.; Yu, L.; Ahamad, T.; Ma, Z. Refined microstructure and enhanced mechanical properties in Mo–Y₂O₃ alloys prepared by freeze-drying method and subsequent low temperature sintering. *J. Mater. Sci. Technol.* **2021**, *88*, 36–44. [[CrossRef](#)]
19. Guo, Y.; Tian, J.; Xiao, S.; Xu, L.; Chen, Y. Enhanced creep properties of Y₂O₃-bearing Ti-48Al-2Cr-2Nb alloys. *Mater. Sci. Eng. A* **2021**, *809*, 140952. [[CrossRef](#)]
20. Chimi, Y.; Iwase, A.; Ishikawa, N.; Kobiyama, M.; Inami, T.; Okuda, S. Accumulation and recovery of defects in ion-irradiated nanocrystalline gold. *J. Nucl. Mater.* **2001**, *297*, 355–357. [[CrossRef](#)]
21. Tong, L.B.; Li, Y.H.; Meng, F.L.; Tian, H.W.; Zheng, W.T.; Wang, Y.M. Investigation on mechanical properties of sputtered TiNi thin films. *J. Alloys Compd.* **2010**, *494*, 166–168. [[CrossRef](#)]
22. Ma, E. Instabilities and ductility of nanocrystalline and ultrafine-grained metals. *Scr. Mater.* **2003**, *49*, 663–668. [[CrossRef](#)]

23. Zhao, M.; Li, J.C.; Jiang, Q. Hall-Petch relationship in nanometer size range. *J. Alloys Compd.* **2003**, *361*, 160–164. [[CrossRef](#)]
24. Kim, K.K.; Song, J.H.; Jung, H.J.; Choi, W.K.; Park, S.J.; Song, J.H. The grain size effects on the photoluminescence of ZnO/ α -Al₂O₃ grown by radio-frequency magnetron sputtering. *J. Appl. Phys.* **2000**, *87*, 3573–3575. [[CrossRef](#)]
25. Yang, M.; Kim, H.C.; Hong, S.H. Growth of ZnO nanorods on fluorine-doped tin oxide substrate without catalyst by radio-frequency magnetron sputtering. *Thin Solid Film.* **2014**, *573*, 79–83. [[CrossRef](#)]
26. Ma, S.; Xu, B.; Wu, G.; Wang, Y.; Ma, F.; Ma, D.; Xu, K.; Bell, T. Microstructure and mechanical properties of SiCN hard films deposited by an arc enhanced magnetic sputtering hybrid system. *Surf. Coat. Technol.* **2008**, *202*, 5379–5382. [[CrossRef](#)]
27. Song, M.; Sun, C.; Jang, J.; Han, C.H.; Kim, T.K.; Hartwig, K.T.; Zhang, X. Microstructure refinement and strengthening mechanisms of a 12Cr ODS steel processed by equal channel angular extrusion. *J. Alloys Compd.* **2013**, *577*, 247–256. [[CrossRef](#)]
28. Wang, J.P.; Yang, Z.G.; Bai, B.Z.; Fang, H.S. Grain refinement and microstructural evolution of grain boundary allotriomorphic ferrite/granular bainite steel after prior austenite deformation. *Mater. Sci. Eng. A* **2004**, *369*, 112–118. [[CrossRef](#)]
29. di Schino, A.; Kenny, J.M. Grain refinement strengthening of a micro-crystalline high nitrogen austenitic stainless steel. *Mater. Lett.* **2003**, *57*, 1830–1834. [[CrossRef](#)]